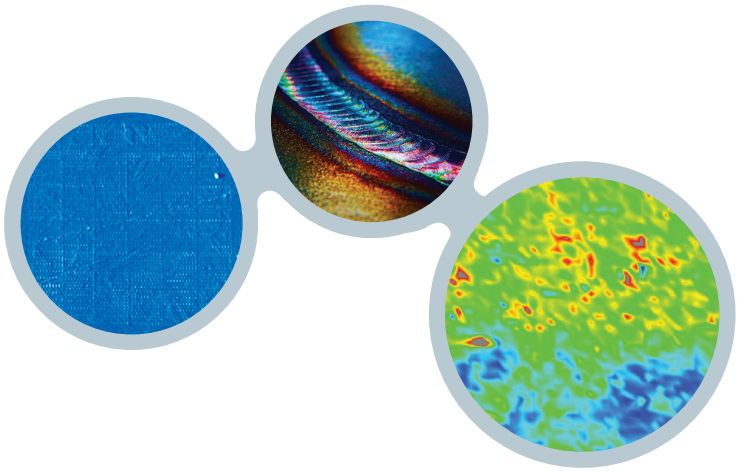

Application Note #1532

Material Joining: Characterization of Laser Beam Welding

Laser beam welding is a modern material joining technique that utilizes a high power density laser to heat and thereby, fuse, two materials together. Compared to traditional welding techniques, laser-based methods can achieve narrower welds, higher speeds and are easier to automate. Like traditional welding techniques, materials are melted in the weld zone, though with much more rapid heating and cooling cycles (see Figure 1). These rapid thermal cycles are potentially concerning for formation cracks through thermal stresses and changes in the microstructure giving undesirable or inhomogeneous mechanical properties. The area in which these microstructural changes occur is referred to as the heat affected zone (HAZ). Thus, high-precision and high-resolution mechanical property data in the HAZ is critical for ensuring weld quality and optimization of laser operating parameters. Laser beam welding is widely used in the automotive and electronic industries where welds are required to be rapid, highly automated, small, and precise. The inherent size of the laser spot size (≈200 µm) used during laser beam welding produces a small HAZ that is often too fine to be properly characterized by optical microscopy and macro/micro indentation techniques like Vickers and Rockwell. A combination of scanning electron microscope (SEM) based characterization techniques and nanoindentation are much better suited to address the length scale of laser beam welds. This application note presents a combined nanoindentation mapping and electron backscatter diffraction (EBSD) study of 410 stainless steel laser cladding on a 4140 steel substrate to evaluate changes in microstructure and mechanical properties as a consequence of the joining process.

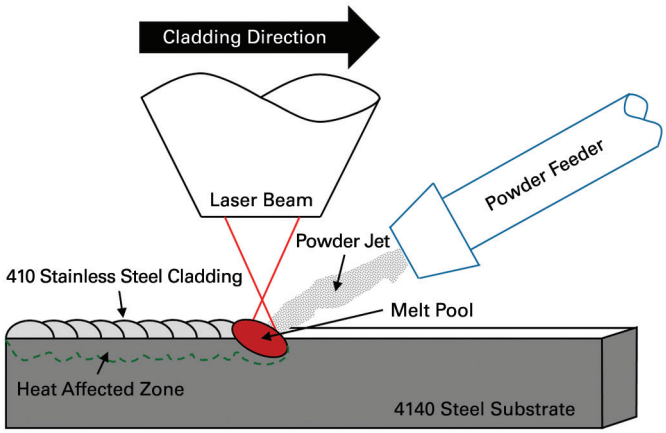

Figure 1. Schematic of laser cladding of 410 stainless steel onto a 4140 steel substrate. The laser beam weld produces a heat affected zone resulting in altered mechanical behavior and microstructure at the weld interface.

Experimental

Nanoindentation experiments were conducted with Bruker's Hysitron® TI 980 TriboIndenter® equipped with a diamond Berkovich probe. A series of quasi-static accelerated property mapping (XPM™) grids with indent spacing of 500 nm over a square distance of 34 µm x 34 µm, at 400 µN force, were carried out to identify the nanomechanical behavior of the weld interface (see Figure 2).

To study the microstructural changes in the steel due to the laser weld, EBSD experiments were conducted using an FEI Versa 3D SEM equipped with a Hikari EBSD detector supplied by EDAX. EBSD maps were gathered

at 20 keV accelerating voltage with a lateral step size of 200 nm. A final polishing step of 50nm colloidal SiO_2 was used for 20 minutes to prepare the surface of the specimen for EBSD analysis. A fiduciary box marking was cut around the area of interest using the focused ion beam with Ga+ ions at 30 keV accelerating voltage and 1 nA beam current to ensure the nanoindentation and EBSD areas were well aligned.

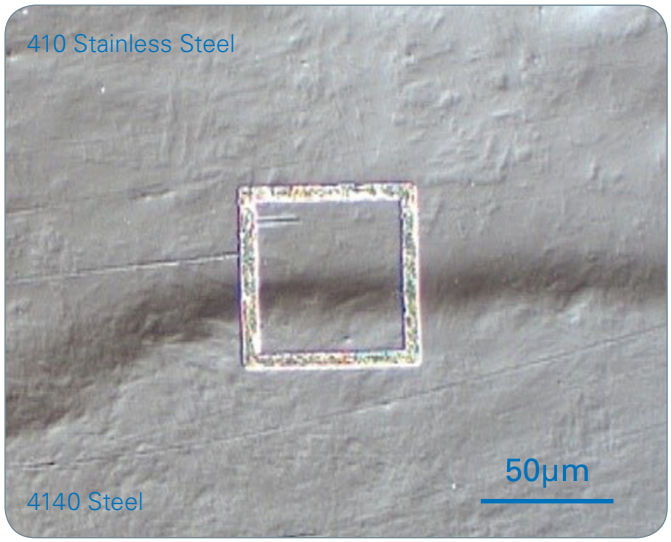

Figure 2. An optical micrograph of a cross-section of a 410 stainless steel/4140 steel laser beam welded interface. Nanoindentation was carried out within the focused ion beam (FIB) ablated square. Note: The nanoindentation grid is not visible.

Results and Discussion

A 2D modulus map of the welded interface is shown in Figure 3a. No spatial variation in elastic properties across the weld are evident; the average reduced modulus was 218.5 GPa ± 17.5 GPa (N=4356 indents). Figure 3b shows the location of the indents within the FIB ablated square. The variation in hardness across the welded interface was apparent with the 4140 steel measuring ≈5 GPa hardness whereas the hardness of the 410 stainless steel was ≈8 GPa, as shown in Figure 3c. It also appears that the hardness is slightly higher within the weld zone as a consequence of rapid quenching of these martensite-hardened alloys.

In Figure 4, these hardness and modulus maps are compared against the EBSD data. The EBSD phase content was measured to be nearly completely alpha phase ferrite (~85%), with well distributed martensite (~7%) and cementite (8%). In Figure 4c, the EBSD inverse pole figure (crystal orientation) map is shown, while in Figure 4d, an image quality map with marked boundaries is shown. The inverse pole figure, Figure 4c, indicates some changes in grain size, shape and relative orientation across the weld zone. The 410 stainless steel possesses slightly smaller

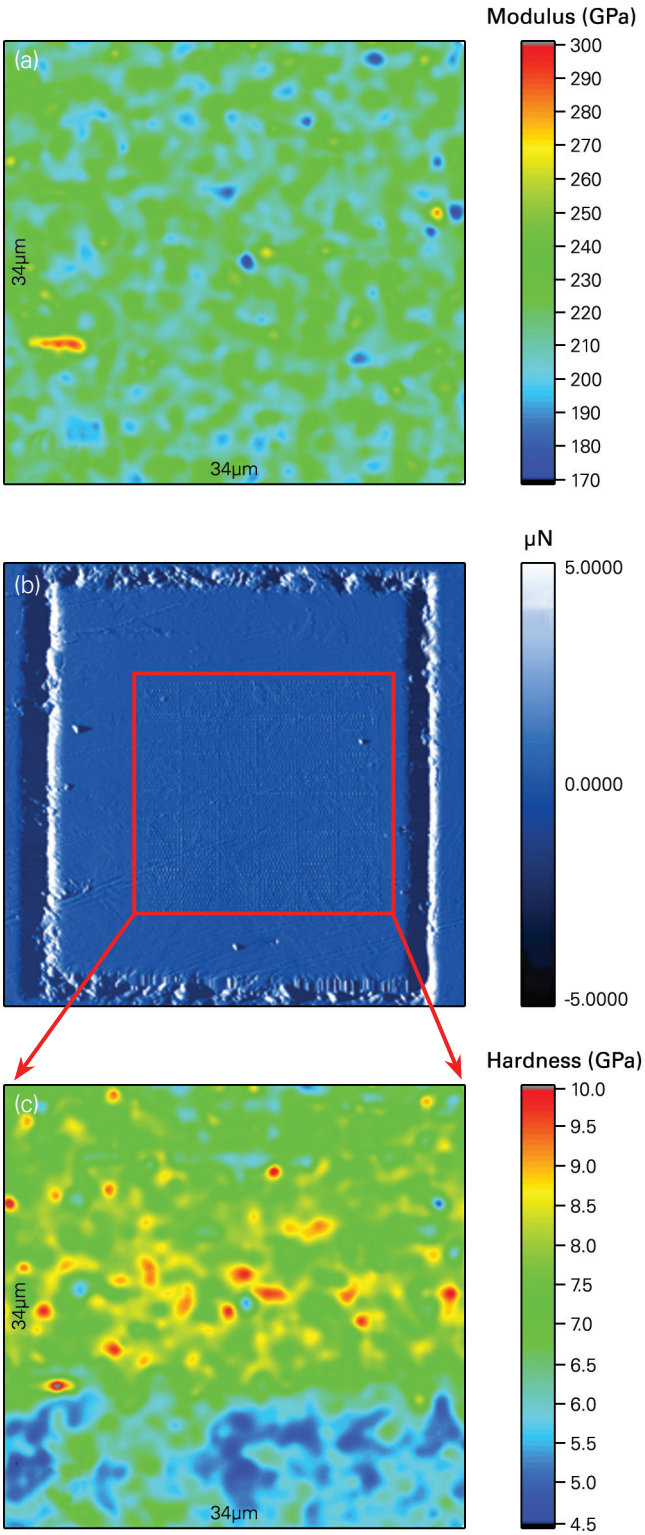

Figure 3. (a) 2D reduced elastic modulus map of the welded interface; (b) location of indents within the FIB ablated square from Figure 2; and (c) hardness map across the welded interface showing distinct differences between the 410 stainless steel and 4140 steel.

and less elongated grains, but much larger orientation changes between neighboring grains, compared to 4140 steel substrate. Thus some of the hardness increase in the 410 can be attributed to a reduced grain size through the Hall-Petch relationship, which states grain size is inversely proportional to yield strength (correlated to hardness).

In addition to differences in grain sizes, Figure 4d shows an increased density of greater than 15° crystal misorientation grain boundaries within the 410 stainless steel compared to the 4140 steel substrate. The higher angle grain boundaries are much more effective at inhibiting dislocation motion. The increased density of greater than 15° misorientation not only supports a difference in grain size between the material types, but also suggests that transmission of dislocations to the neighboring grain is more difficult, increasing dislocation pile up sizes and dislocation-dislocation interaction based hardening.

Conclusions

The combined XPM nanoindentation and EBSD mapping demonstrated correlated structure property relationships in this stainless steel-steel weld zone, where higher hardness was attributed to decreased grain size and increased average grain boundary angle. Overall, the weld zone was fairly structurally homogenous, but possessed some areas of high local hardness. The speed of XPM mapping allowed nearly 5000 indents to be performed in roughly 30 minutes, with comparable speed and resolution to the EBSD mapping.

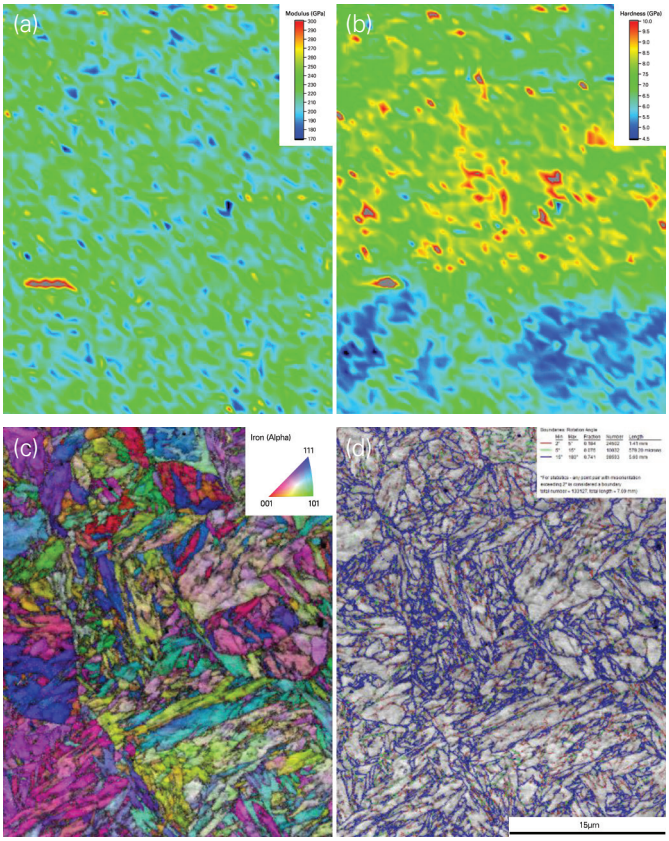

Figure 4. (a) Modulus map; (b) hardness map; (c) EBSD inverse pole figure map (i.e., crystal orientation); and (d) EBSD image quality map (i.e., crystal misorientation/grain boundary).

Authors

Eric Hintsala (eric.hintsala@bruker.com)
Jared Risan (jared.risan@bruker.com)
Bruker

John Haake
Titanova, Inc.

Hysitron, TriboIndenter, and XPM are trademarks of Bruker Corporation. All other trademarks are the property of their respective companies.
© 2019 Bruker Corporation. All rights reserved. AN1532, Rev. A0

Bruker Nano Surfaces Division
Minneapolis, MN · USA
+1.952.835.6366
productinfo@bruker.com

www.bruker.com/nanomechanical-testing